

Meson decay in $e p \rightarrow e p K^+ K^-$ and $e p \rightarrow e p K^+ K^- \pi^0$ events

By

Patrick Walker

has been approved

Spring 2021

APPROVED (printed name, signature):

Michael Dugger

Thesis Director

Maxim Sukharev

Second Committee Member

ACCEPTED:

Dean, Barrett, The Honors College

Background

Within the realm of particle physics, the quark model is accepted as the scheme for classification of hadrons in general and mesons in particular. Mesons are not considered to be elementary particles; they are bound states of their quark and antiquark pairs, which relates directly to their quantum numbers. All mesons are unstable and decay very quickly, where the heavier mesons often decay into lighter mesons, and the lighter mesons decay into stable particles such as electrons, photons, and neutrinos. Because mesons consist of a quark antiquark pair, each meson has an antiparticle where quarks are replaced by antiquarks and vice versa with a few mesons being their own antiparticle. For instance, a positive Kaon K^+ has a composition of one up quark and one strange antiquark ($u\bar{s}$), while the antiparticle K^- has a composition of one up antiquark and one strange quark ($s\bar{u}$). Since quarks are spin $\frac{1}{2}$ particles, mesons can exhibit the spin-1 triplet, or the spin-0 singlet [1]. The spin S and orbital angular momentum L add to form the total angular momentum J , that can assume values from $J = |L - S|$ up to $J = |L + S|$ and are analyzed to allow the classification of these particles [1].

The main classification of the quantum numbers of mesons would be the Poincaré symmetry, J^{PC} , where J represents the total angular momentum, P represents P-symmetry, and C represents C-symmetry. $P = (-1)^{L+1}$ is a spatial parity conserved in non-weak physical interactions; this emphasizes the product of the intrinsic parities are the same before and after the reaction [2]. $C = (-1)^{L+S}$ is representative of the charge conjugation symmetry where the charge conjugation switches all particles with corresponding antiparticles [2]. This charge conjugation represents whether the meson wavefunction stays the same or inverts when the meson quarks are conjugated. The meson is “even” if the wavefunction is equivalent after the conjugation, and “odd” if the conjugated wavefunction is equal to the negation of the original

wavefunction. This is only applicable to mesons that are their own antiparticle— such as π^0 — since conjugating the quark and antiquark results in the antiparticle’s configuration. Mesons exist in the following J^{PC} states:

$$0^+, 0^{++}, 1^-, 1^+, 1^{++}, 2^-, 2^+, 2^{++}, 3^-, 3^+, 3^{++}, \dots$$

Based on the Quark Model there are certain J^{PC} quantum numbers that are not allowed for mesons which are:

$$0^-, 0^{+-}, 1^+, 2^+, 3^+, 4^+, \dots$$

Observing any of these states highlights there is something outside the simple quark model. These states can include sets of two or three gluons – glueballs, multi-quark states like tetraquarks ($q\bar{q}q\bar{q}$), or hybrid mesons ($q\bar{q}g$) [2]. Hybrid mesons are quark-antiquark pairs that have one or more gluons and occur when an excitation of a gluonic field binds to the quark-antiquark. Since gluonic fields can carry quantum numbers that differ from a vacuum, the gluonic field binding one or more gluons to the meson can change the J^{PC} value. One of the more researched states is 1^{+-} hybrid which theories predict hybrid meson states π_1 , η_1 , and η'_1 , with the lightest state being π_1 , and η'_1 being the heaviest 1^{+-} [3]. There is experimental evidence pointing towards π_1 existence with a mass around 1400 MeV with observed decays of $\eta\pi$ [4]. Theories for η'_1 suggest that this particle is a promoted gluon hybrid that decays K^*K .

Experiment

The CLAS12 Detector shown in Figure 1, located in the Jefferson Laboratory experimental Hall B, implements the use of a 0.5 to 12 GeV electron beam that is generated within the accelerator of Jefferson Laboratory. The electrons in the incoming beam collide with nuclei of atoms known as the target which is considered the center of the detector, since all scattering of interest originates when the electron beam encounters the target. This high energy

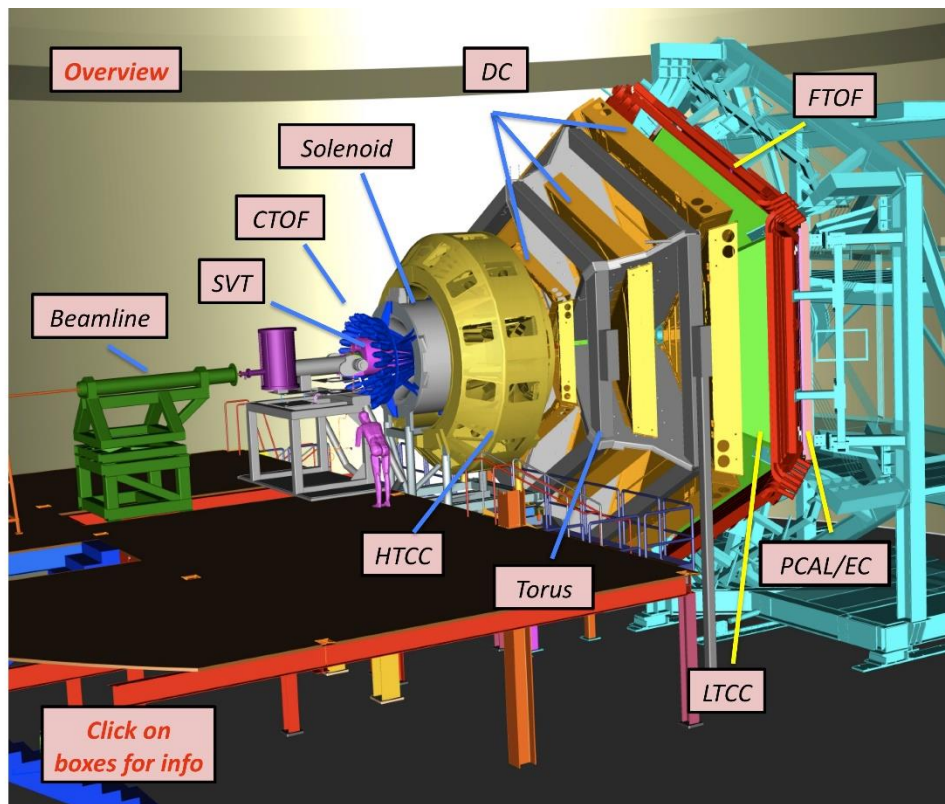


Figure 1: CLAS12 Detector

collision causes hadrons to appear for a short time before decaying. Electrons and longer living particles can pass through the detector where they are sorted out and measured. The detector takes each particle from a target collision to form an event, and with the detector running there can be multiple thousands of events per second. Many events are needed to reduce the statistical uncertainty in the measurement.

The Central Time-of-Flight (CTOF) shown in Figure 2 measures time-of-flight in the central region of the CLAS12 detector. This detector consists of 48 scintillating counters arranged in a hermetic barrel aligned with the axis of the beamline. Located within the solenoid

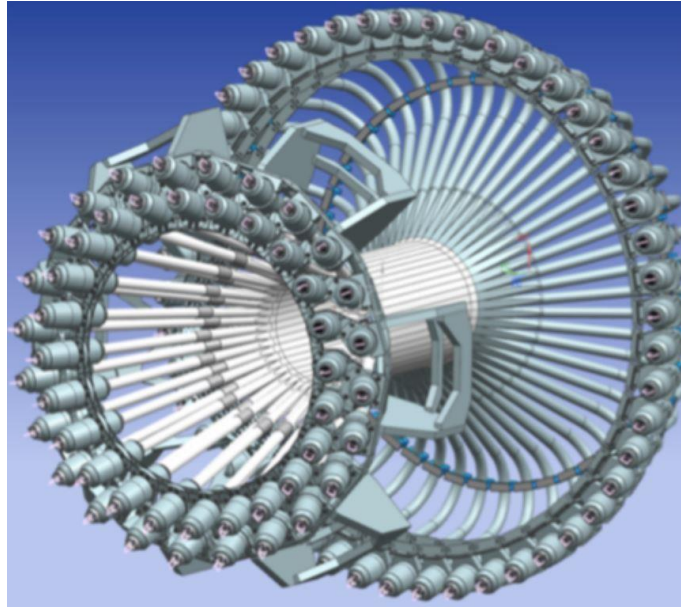


Figure 2: Central Time of Flight

between the Central Vertex Tracker and Central Neutron Detector, the CTOF assists in the identification of charged particles with a goal resolution of 50-60 ps but required resolution of 65 ps. This allows for the detector to see a separation of up to 0.64 GeV/c between pions and kaons. The CTOF detects charged particles within a range of $35^\circ < \theta < 135^\circ$ [5]. With photomultipliers on both ends of the CTOF, the timing from upstream and downstream photomultipliers are used to determine the time that a charged particle passed through the detector.

The Silicon Vertex Tracker (SVT) shown in Figure 3 is located in the central tracking system centered inside the solenoid. The SVT allows for momentum tracking up to 1 GeV with a momentum resolution less than or equal to 5%. The SVT is divided into 4 regions with each

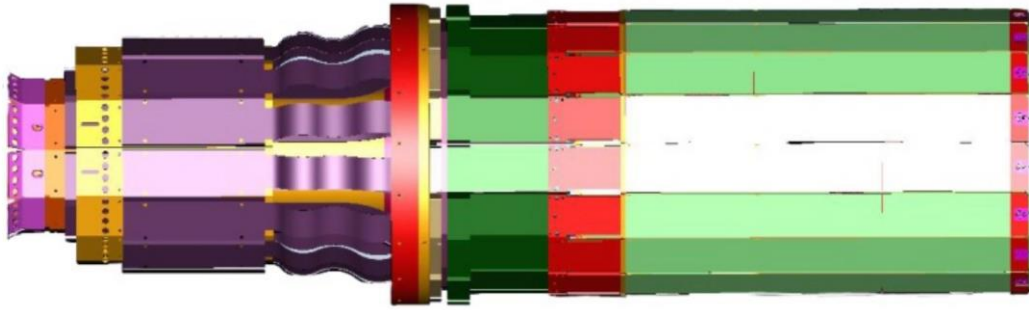


Figure 3: Silicon Vertex Tracker

sector containing regions of different radial lengths containing 10, 14, 18, or 24 double-sided silicon sensors. The innermost region has a radius of 65mm, while the next is 93mm, followed by a region at 120mm, and last, a radius of 161mm for the outer. This configuration allows for high luminosity processes ($L = 10^{35} \text{ cm}^2 \text{ s}^{-1}$) that are required for these reactions. Since the primary purpose is to measure pions and kaons at large angles along with baryons that recoil, the SVT evaluates the vertex of charged particles passing through the target at $\theta = 90^\circ$ [5]. Matching tracks and hits with the CTOF, the SVT aids with the goal resolution of the CTOF.

The Forward Time-of-Flight (FTOF) shown in Figure 4 is a system implemented to measure the time-of-flight of charged particles emanating from the target in the forward direction. The system is split into 6 sections with each section having plastic scintillators with double-sided photomultipliers along each section. Each of the 6 sections are split into three different arrays for counting: panel-1a with 23 counters, panel-1b with 62 counters, and panel-2

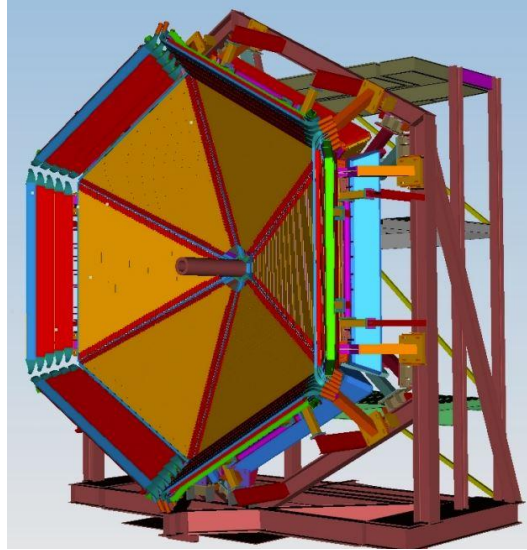


Figure 4: Forward Time of Flight

with 5 counters. Each panel has a different design and goal resolution, along with varying dimensions to cover angles between $5^\circ < \theta < 45^\circ$. This design meets the requirements needed for timing resolutions which assists in particle identification. For pions and kaons, the FTOF can separate the two particles momentum up to 2.8 GeV/c. With kaons and protons, there is a separation of up to 4.8 GeV/c, while pions and protons have a separation of up to 5.4 GeV/c [5]. This separation allows for clearer identification of these charged particles.

The High Threshold Cerenkov Counter (HTCC) shown in Figure 5 – integrated specifically for electron beam experiments – is employed to get fast trigger signals. This works by the system having a high rejection of charged π -mesons to create a low background noise that allows for the maximization of scattered electron detection. The HTCC uses 60 lightweight multifocal mirrors that are ellipsoidal which focus Cerenkov light onto each of the 5-inch

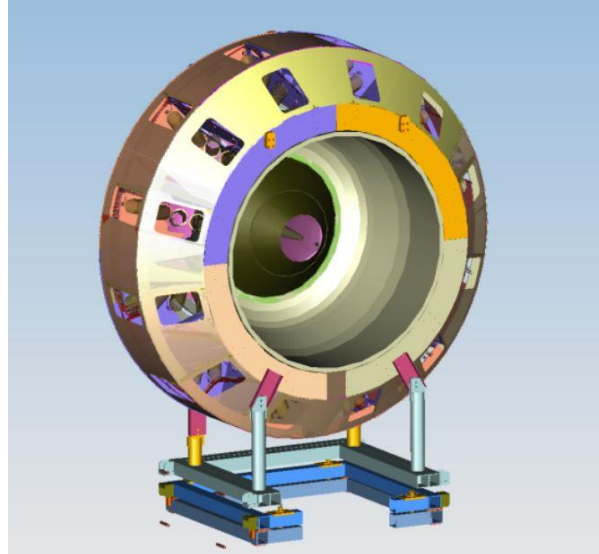


Figure 5: High Threshold Cerenkov Counter

phototubes. It is designed for filtration of all pions at 2 and 4 GeV/c [5]. This high rejection of the pions allows for up to 99.9% electron detection efficiency while minimizing background noise.

Within the CLAS12 detector, there are two major electromagnets the Solenoid and Torus. The Solenoid is located around the beam line – producing a field primarily in the direction of the beam and allows tracking for central particles in the detector. The solenoid has four coils as the main core with a total of 3704 turns and a shielding coil with 1392 turns. This solenoid has a nominal current of 2416 amperes of current which can produce a 5-tesla central magnetic field with a peak of 6.56-tesla. This creates a nearly symmetric magnetic field around the beamline which allows for accurate operations with the target. The Torus magnet (centered around the

beam line but radially outward from the Solenoid) produces a field primarily in the azimuthal direction. The Torus creates an approximate toroidal field distribution centering on the beamline. Consisting of six coils each with 234 turns, the Torus has a nominal current of 3770 amperes which creates a peak magnetic field of 3.58 tesla. This Torus has a large acceptance of particles traveling in the forward path but only a 50% particle acceptance at 5 degrees from the beam axis. Furthermore, the Torus has an open bore design to allow scattered particles to pass through [5]. This design is needed because of the Torus's location between two different Drift Chambers, so there needs to be a high capacity of charged particles making it through the Torus.

The Low Threshold Cerenkov Counter (LTCC) shown in Figure 6 is a part of the forward detection for the CLAS12 detector and is used primarily for discriminating between pions and

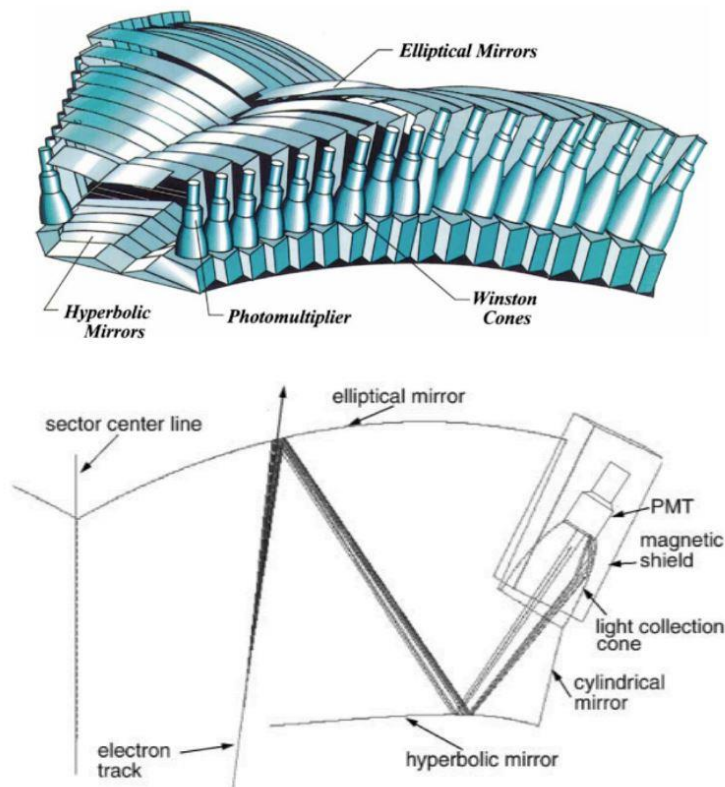


Figure 6: LTCC Design and Interior Optics

kaons. This system contains 6 sectors each containing 36 light collection or Winston Cones, 108 lightweight mirrors that are either elliptical, cylindrical, or hyperbolic, 36 5-inch

photomultipliers, and magnetic shielding. Each of these sectors are filled with Perfluorobutane which is chosen for its refraction index of 1.00134 and 100% transparency for light with wavelengths above 220 nanometers. The mirrors are positioned with elliptical mirrors radially outward of the hyperbolic mirrors. This allows for the electron track to first contact the elliptical mirror – causing it to scatter and reflect into the hyperbolic mirror. From there, the scattered electron track is focused into the photomultiplier through the light collection cone [5]. This design allows for a goal pion kaon separation of 3.5 GeV/c, but it can track up to a 9 GeV/c separation.

The Drift Chambers shown in Figure 7 are wire chambers measure the momentum of charged particles in the detector. Located at the back of the detector. There are 18 chambers divided into three regions which consist of 24,192 sensor nodes. The first region begins one

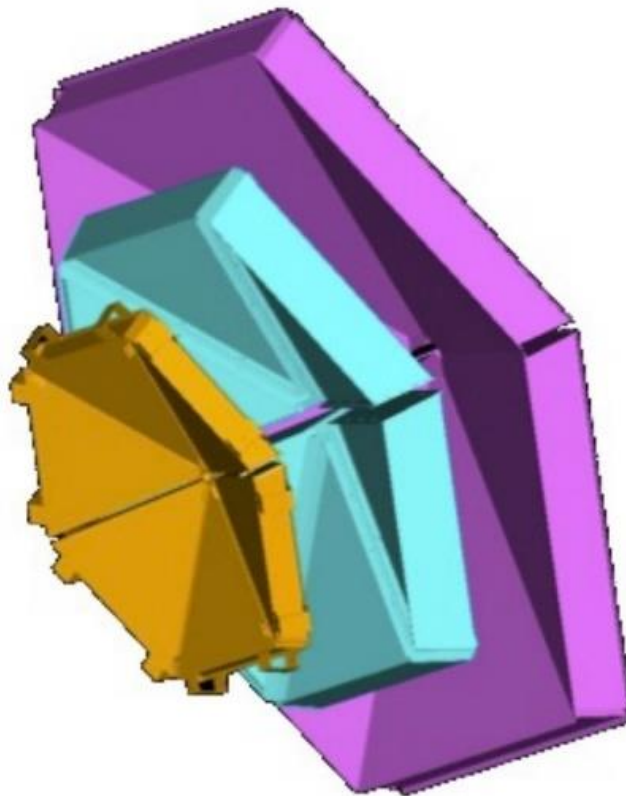


Figure 7: Drift Chambers

meter radially away from the target, while the second chamber – located within the torus – sits two meters away, while the third region is one meter radially behind the torus. These Drift Chambers operate on high and low voltage signals and give a spatial resolution of 250 – 350 micrometer which meets the requirements needed for momentum resolution. Within each Drift Chamber is a gas mixture of 90:10 Argon to Carbon Dioxide which is constantly monitored by epics. Epics control over and under pressure relief valves to keep the gas ratio as constant as possible while runs on the detector are made. With its current design, the Drift Chambers have an angular coverage of $5^\circ < \phi < 40^\circ$ with only 50% coverage at $\phi = 5^\circ$. This helps to achieve the high luminosity process with a momentum resolution of less than 1% [5]. The Drift Chambers are mostly used to distinguish charged particles from one another so the Electric Calorimeter can have reasonably clear data.

Behind the Drift Chambers exist the pre-shower calorimeter (PCAL) and the electromagnetic calorimeter (ECAL) – where both calorimeters together are known as the EC Detector. The PCAL is placed 7 meters away from the target while the ECAL is placed 7.5 meters from the target which means that these devices are the furthest away from the beamline. These two systems work in tandem to identify charged particles with emphasis on $\pi^0 \rightarrow \gamma\gamma$ decay. Each piece consists of six triangular modules formed by layering 54 1-cm thick scintillators placed between 2.2-mm thick lead sheets. The scintillator layers are combined into three readout groups: PCAL, ECAL-inner, and ECAL-outer. The PCAL geometry covers a 45 meter square area while the ECAL has a 49 meter square area. Each device has photomultiplier readout for photons that reach the EC Detector [5].

Software

Data collected from the CLAS12 particle detector in search of these exotic meson states was analyzed. For the data analysis, ROOT was implemented, a program developed by CERN that aids in visualizing large amounts of data, designed specifically for particle physics data analysis. ROOT implements a tree data container which has substructures of branches and leaves, designed to aid in memory allocation when working with large data sets. This tree structure allows for quick access to specific places within the data. ROOT is written in C++ and all manipulation and analysis of data with these files was through the C++ language. ROOT was implemented on a Linux virtual machine since Linux is a developer focused operating system that allows for easy integration between the C++ and ROOT files. ROOT contains all the data within its tree structure, then with implementation of C++ code one can gather and organize data into various histograms which ROOT is employed for visualization. Once the histograms are displayed in ROOT, I implement other aspects of this program for data analysis such as plot fitting are utilized. ROOT can easily fit and manipulate data and was used throughout the analysis.

Analysis

The data analyzed from the CLAS12 detector is a combination of data from 173 individual runs. From this data, I begin by identifying light mesons that will enable us to build

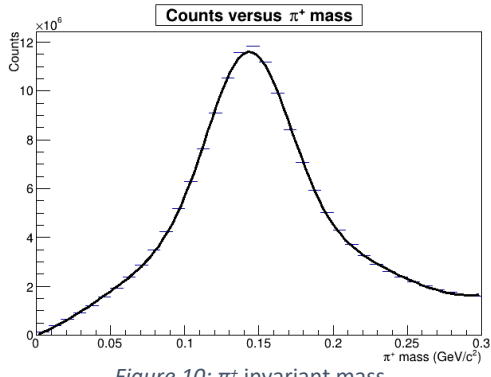


Figure 10: π^+ invariant mass

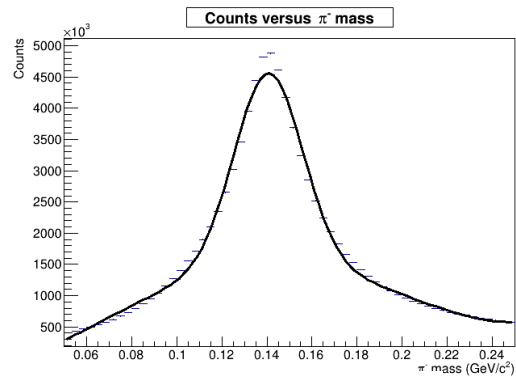


Figure 11: π^- invariant mass

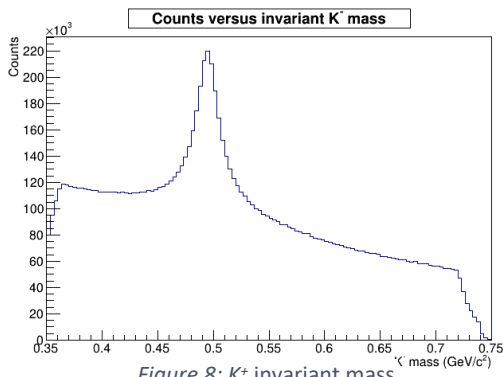


Figure 8: K^+ invariant mass

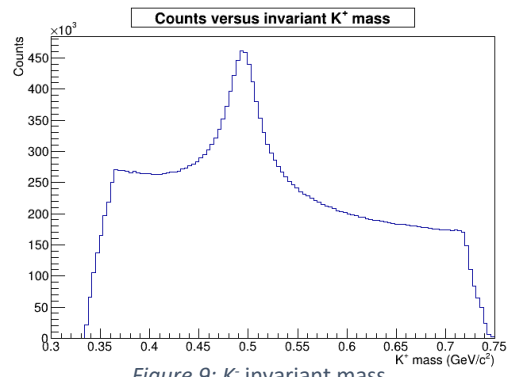


Figure 9: K^- invariant mass

reactions based on known decay modes to search for heavier meson states. Figures 8—11 show plots of these lighter meson states: K^+ , K^- , π^+ , and π^- . These particles are relatively easy to uncover within the data since the CLAS12 detector is built specifically to distinguish lighter

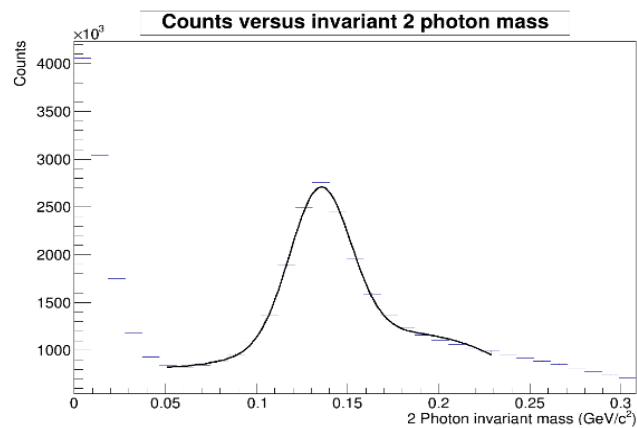


Figure 12: 2 photon invariant mass with π^0 fit

mesons from each other. Other mesons are discovered within reactions based on how they decay like π^0 which usually decays into two photons ($\pi^0 \rightarrow \gamma\gamma$). Therefore, taking a plot of two photons' invariant mass – shown in Figure 12 – reveals a peak around $0.14 \text{ GeV}/c^2$ that is the π^0 meson. These mesons are used to look for heavier mesons that decay into them.

The initial reaction looked at is $e p \rightarrow e p K^+ K^-$. A lot of mesons have a decay of $K^+ K^-$ which makes this reaction a good starting point for further evaluation. Plotting the invariant mass of $K^+ K^-$, the $\phi(1020)$ shows up as a small peak around $1 \text{ GeV}/c^2$ in Figure 13. This peak is visible but not well defined for the meson, so data cuts are made based on physical assumptions

about the reaction. The first cut made to the data was based on a missing mass plot. Looking at a similar reaction $e p \rightarrow e p K^+ K^- X$, where X should be zero, a graph of the $(\text{mass of } X)^2$ is created. All that is not within three standard deviations of zero

are cut. This plot – shown in Figure 14 – cuts a lot of events, and cleans up the ϕ peak, which can clearly be seen in Figure 15. The peak for $\phi(1020)$ is more

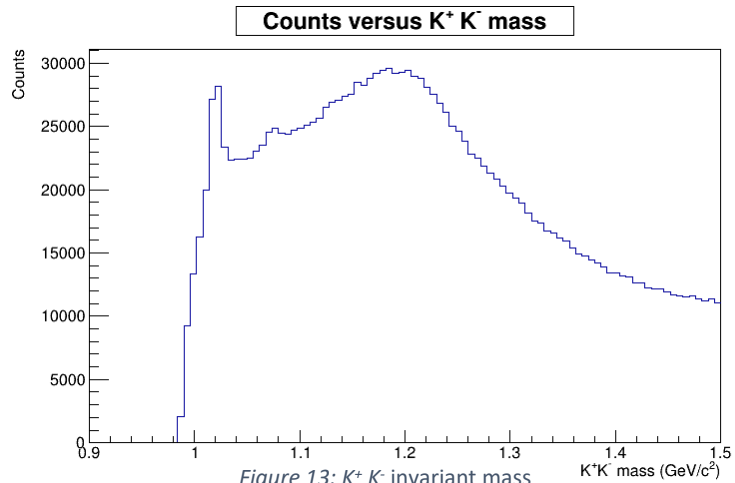


Figure 13: $K^+ K^-$ invariant mass

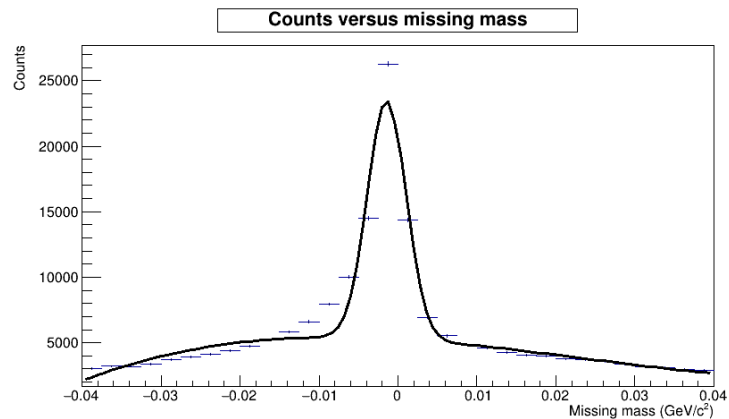


Figure 14: X invariant mass²

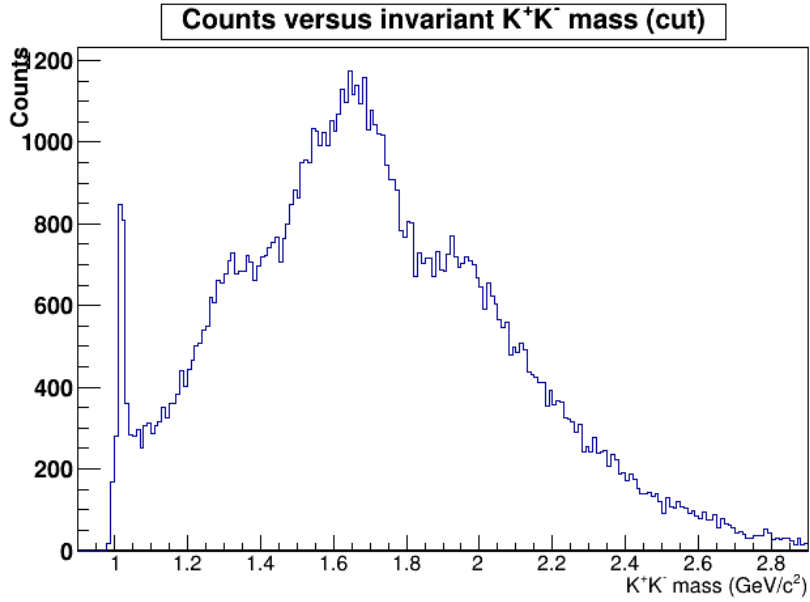


Figure 15: $K^+ K^-$ invariant mass after missing mass cut

distinguished and visible for this meson. Another place to look for baryonic states within the same reaction is with an invariant mass plot of $p K^-$. The same missing mass cut can be applied to this plot which reveals two different peaks shown in Figure 16: the first around 1.5 GeV/c^2

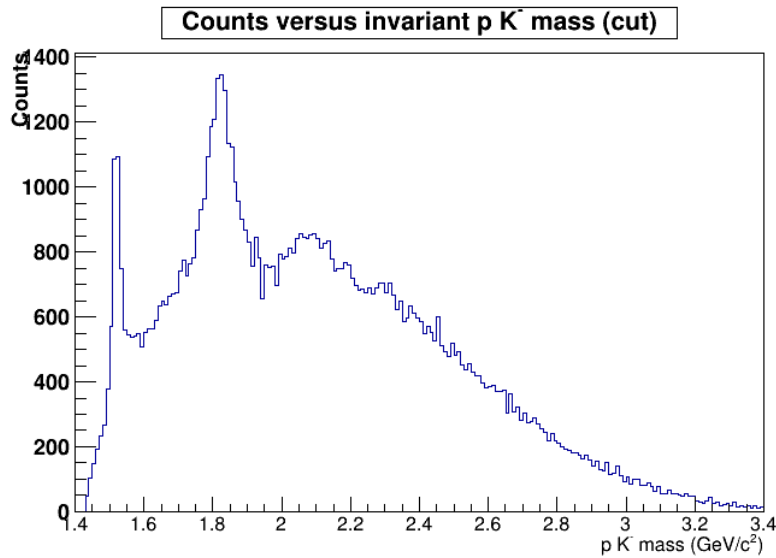


Figure 16: $p K^-$ invariant mass after missing mass cut

which is $\Lambda(1520)$ and the second around 1.8 GeV/c^2 which is a combination of $\Lambda(1800)$, $\Lambda(1810)$, $\Lambda(1820)$, and $\Lambda(1830)$.

The next step was the addition of π^0 into the reaction: $e p \rightarrow e p K^+ K^- \pi^0$. Initially, there was no distinguishable peaks. Within in the beta versus momentum plot of the K^+ and K^-

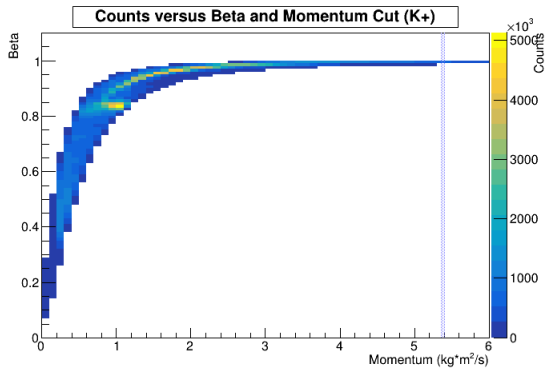


Figure 17: Beta versus momentum K^+

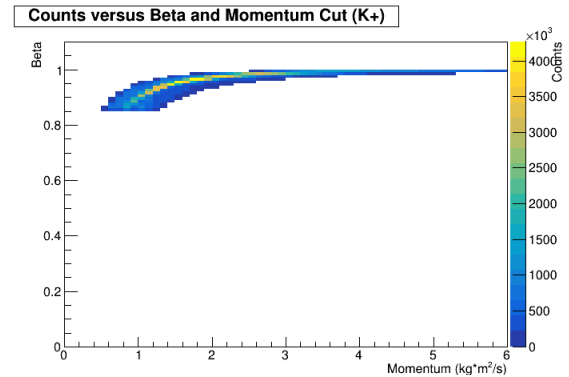


Figure 18: Beta versus momentum K^+ after beta cut

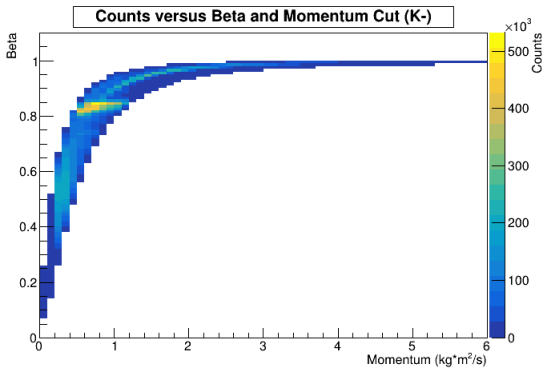


Figure 19: Beta versus Momentum K^-

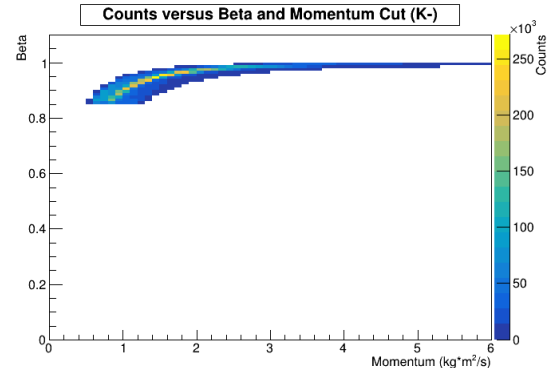


Figure 20: Beta versus momentum K^- after beta cut

mesons, which can be seen in Figures 17 and 19 as a horizontal stripe, appearing at $\beta = 0.855$ in both figures. All kaons with a beta value less than 0.855 were cut, with the resulting Beta versus momentum plots shown in Figures 18 and 20. These particles with $\beta < 0.855$ needed to be cut

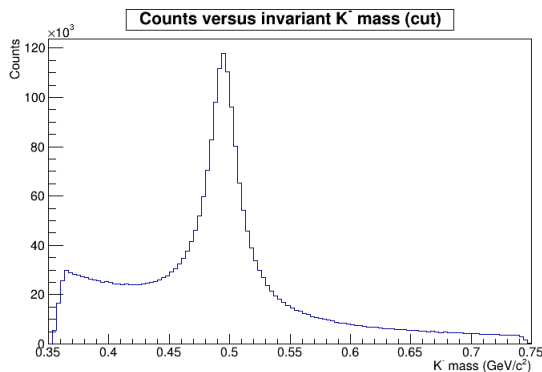


Figure 21: Invariant K^- mass after beta cut

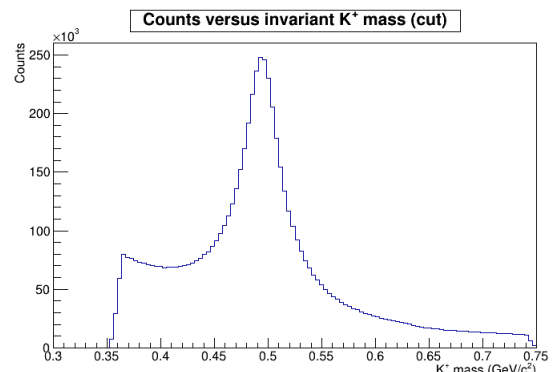


Figure 22: Invariant K^+ mass after beta cut

out of the data because of possible contamination where particles that are not kaons could possibly show up in this spectrum. These kaon cuts take a lot of events away, so the particle

identification for K^+ and K^- is checked to make sure nothing drastic has changed. These beta cuts help diminish the background for the Kaons' invariant mass plots which Figures 21 and 22 highlight. Now that the beta cut did not negatively impact the mass plots, the invariant mass of $K^- \pi^0$ shown in Figure 23 is investigated. There is now a distinguished peak around $0.9 \text{ GeV}/c^2$,

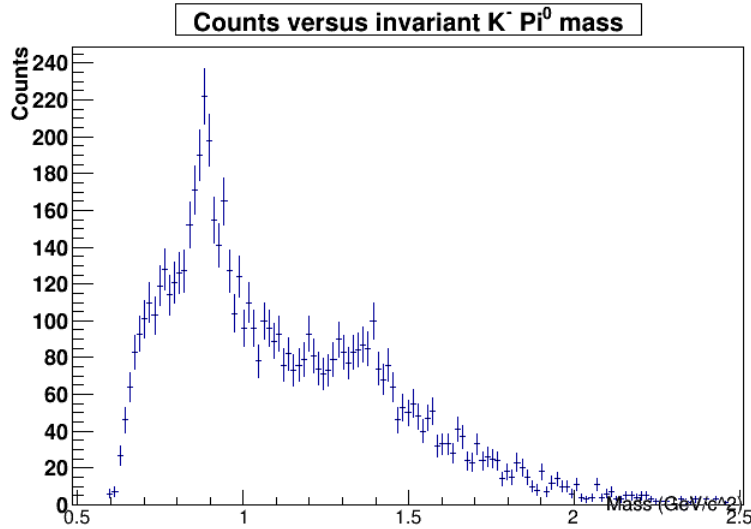


Figure 23: Invariant $K^- \pi^0$ mass after beta cut

identified as $K^{*}(892)$. Next, an invariant mass plot of $K^+ K^- \pi^0$ with restrictions on the $K^- \pi^0$ mass to be between 1.25 and $1.5 \text{ GeV}/c^2$ is plotted. There is a peculiar peak on this graph around $1.94 \text{ GeV}/c^2$ which has no relevant particle identification within the Particle Data Group for this

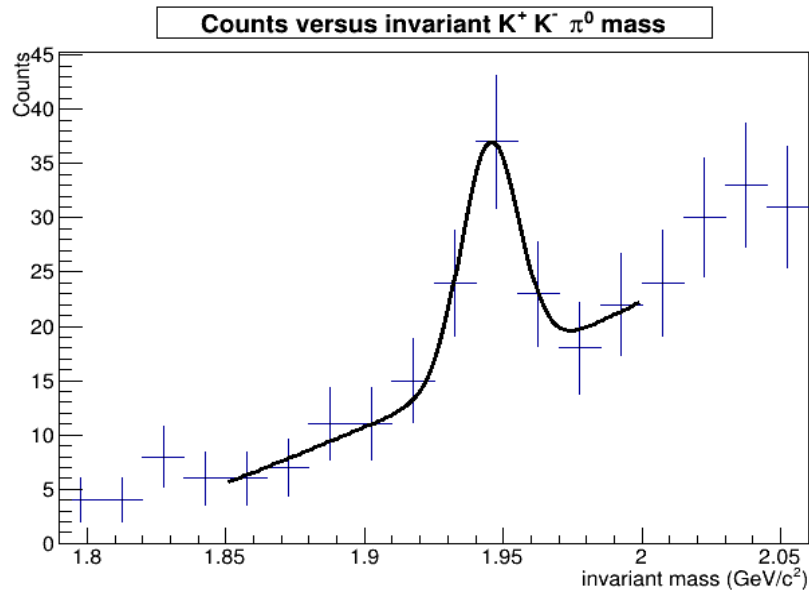


Figure 24: Invariant $K^+ K^- \pi^0 (K^{*}(1430) K)$ mass

decay channel. Figure 24 shows the invariant mass plot with a fit of this unknown peak. The next step is to check for statistical anomalies since this data set has limited statistics. A beta cut for Kaons was made, so kaons now only exist within the range: $0.855 < \beta < 0.98$. Another data cut made was limiting the momentum of kaons to be less than 3 GeV/c. With both cuts made, the peak was diminished, but still there as seen in Figure 25. Even though it looks as if there is something there, more statistics are required to be certain. Better statistics that should be available via a scheduled run on the CLAS12 detector for newer and cleaner data on this interaction. If this particle at $1.94 \text{ GeV}/c^2$ exists there must be a working J^{PC} value to go along

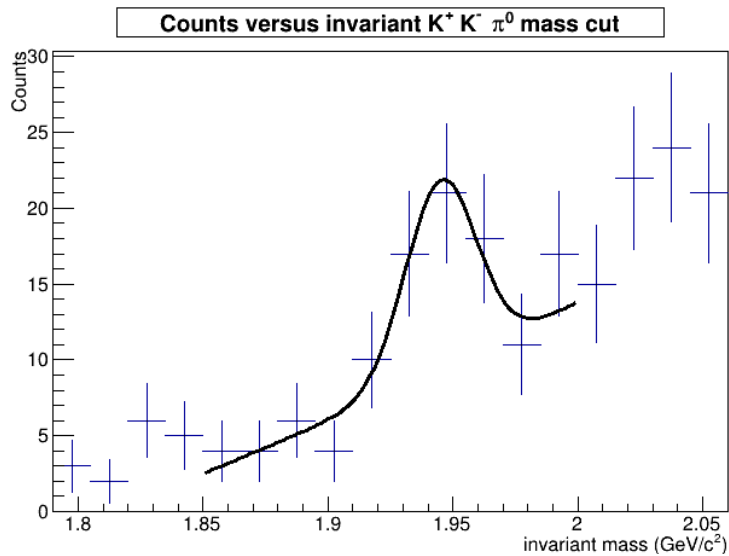


Figure 25: Invariant $K^+ K^- \pi^0 (K^*(1430) K)$ mass after cuts

with it. However, this is a case where there is not enough statistics to begin working through the calculations needed to determine each value. Once more statistics are available, it should be possible to determine the angular momentum by creating a Feynman Diagram for the particle interaction and working through the mathematics for each of the vertices.

References

- [1] R. August, C. Amsler, S. Meyer, T.D.C. U, 15 . Quark Model, 030001 (2019) 1–29.
- [2] GlueX Physics Exotic Quantum Number Mesons, (n.d.).
https://halldweb.jlab.org/wiki/index.php/GlueX_Physics_Exotic_Quantum_Number_Mesons.
- [3] C.A. Meyer, E.S. Swanson, Hybrid mesons, Prog. Part. Nucl. Phys. 82 (2015) 21–58.
<https://doi.org/10.1016/j.pnpnp.2015.03.001>.
- [4] M. Dugger, B. Ritchie, E. Anassontzis, P. Ioannou, C. Kourkoumeli, G. Voulgaris, N. Jarvis, W. Levine, P. Mattione, C. a Meyer, R. Schumacher, P. Collins, F. Klein, D. Sober, D. Doughty, a Barnes, R. Jones, J. McIntyre, F. Mokaya, B. Pratt, I. Senderovich, W. Boeglin, L. Guo, P. Khetarpal, E. Pooser, J. Reinhold, H. Al Ghoul, S. Capstick, V. Crede, P. Eugenio, a Ostrovidov, N. Sparks, a Tsaris, D. Ireland, K. Livingston, D. Bennett, J. Bennett, J. Frye, J. Leckey, R. Mitchell, K. Moriya, A study of meson and baryon decays to strange final states with GlueX in Hall D, (2012) 1–20.
- [5] CLAS12, Jefferson Lab. (n.d.). <https://www.jlab.org/physics/hall-b/clas12>.